PETROLOGY OF YAMATO-791493, "LODRANITE": MELTING, CRYSTALLIZATION, COOLING HISTORY, AND RELATIONSHIP TO OTHER METEORITES

Hiroko NAGAHARA and Kazuhito OZAWA

Geological Institute, University of Tokyo, 3-1, Hongo 7-chome, Bunkyo-ku, Tokyo 113

Abstract: Yamato-791493 is a unique meteorite which is similar to Lodran, an associated "stony-iron" meteorite, but it differs from Lodran in that it contains plagioclase. Y-791493 consists of small spinel, large euhedral to subhedral olivine and orthopyroxene, anhedral clinopyroxene, metallic iron-nickel, troilite, plagioclase, and merrillite. Textural and petrofabric studies show that Y-791493 was not formed by an accumulation of crystals on the stagnant floor of a reservoir but was formed in the presence of strong magmatic laminar flow. Y-791493 cooled continuously from high temperature (above 1200°C) to low temperature (below 500°C) without any thermal interruption. The estimated cooling rate from 800 to 600°C is 10^3 °C/Ma. Orthopyroxene and clinopyroxene show compositional zoning formed during cooling from about 1100 to 800°C. The composition of spinel shows a strong size dependence due to differences in crystallization (Al, Cr, and Ti) and in subsolidus equilibration (Mg and Fe). Similarity in major element abundances to H-chondrites suggests that the precursor material of Y-791493 was similar to the average H-chondrite but was more enriched in Mn and P. Y-791493 was formed by partial melting of the precursor material, followed by crystallization of major portion with minor loss of partial melt under more reduced conditions than the average H-chondrite. From the bulk major chemical and mineralogical similarities, it is suggested that Y-791493 has an intimate genetical relationship to the Lodran, Acapulco, and ALH-77081 meteorites, and probably to "winonaites", Brachina, and silicates in IAB and IIICD irons. These meteorites were formed from a common precursor material in the same parental body, but by different degree of melting. Lodran is a product of the largest degree of melting followed by Y-791493 and Acapulco or ALH-77081.

1. Introduction

Yamato-791493 was once classified as a "lodranite", a stony-iron meteorite (PRIOR, 1916; WASSON, 1974), and its similarity to three other Antarctic meteorites (Y-74357, Y-75274, and Y-8002, the latter two being paired) was pointed out (YANAI and KOJIMA, 1982, 1983; MATSUMOTO *et al.*, 1983). YANAI *et al.* (1984), however, reclassified Y-791493 and three other related meteorites as "primitive achondrites". The term "primitive achondrite" was proposed by PRINZ *et al.* (1980) for meteorites that have chondritic major bulk chemistry but show achondritic textures, *i.e.*, "winonaites" (Winona, Mt. Morris, Pontlyfni, ALH-77081, Acapulco, and Tierra Blanca") (PRINZ *et al.*, 1980). They further extended the group to include "lodranites",

Brachina, and silicate inclusions of IAB and IIICD irons and called them "modified-primitive achondrites" (PRINZ *et al.*, 1983).

Lodran is a coarse-grained meteorite having metallic iron-nickel, olivine, orthopyroxene in roughly equal amounts with minor amounts of spinel, troilite, and merrillite (BILD and WASSON, 1976; PRINZ *et al.*, 1978). Although it is evident from texture and mineral compositions that Lodran was formed by intensive heating followed by slow cooling, its origin and relationship to other meteorite groups have not been well understood. BILD and WASSON (1976) inferred that Lodran is a residue of partial melting in a parental body, which was formed by accretion of metal and silicates directly condensed from the solar nebula. PRINZ *et al.* (1978) argued that Lodran is a cumulate, but PRINZ *et al.* (1983) proposed a minor partial melting for the formation of Lodran as well as "winonaites", Brachina, and silicates in IAB and IIICD irons.

In order to understand its origin and genetic relationship to other meteorite groups, we have conducted a detailed petrological study of Y-791493. Its crystallization and cooling history are clarified, and chemical and petrological relationships to other related meteorites will be discussed.

2. Experimental Methods

Two polished thin sections of Y-791493 were studied, the first one is Y-791493,91, loand from the National Institute of Polar Research and the second one was newly prepared. After microscopic observation, detailed microprobe work was conducted at the University of Tokyo with JEOL JXA-5 of the Geological Institute and a JEOL JCXA-733 of the Ocean Research Institute. Correction procedures are based on both Bence-Albee (BENCE and ALBEE, 1968) and ZAF methods. The newly prepared thin section was further studied by a computer-aided multi analyzer (CMA, hereafter) by JCMA-733 at the EPMA Application Laboratory of Electron Optics Technical and Engineering Division of JEOL. The entire area of the specimen was analyzed by automatically moving the stage. Operating conditions for the CMA analysis were 15 kV accelerating voltage, 2×10^{-7} A probe current (two orders larger than usual microprobe analyses), 50 ms counting time, 5×4 μm analyzed area for each analysis, and 672×778 total number of analyzed points. Elemental count-rates obtained under these conditions were converted to concentrations according to the calibration curves determined from several representative analyses on the specimen. The results are shown as colored maps, where elemental concentration or cation ratios are arbitrarily divided into eight groups shown by different colors.

3. Texture

Y-791493 is a coarse-grained rock consisting of olivine, orthopyroxene, clinopyroxene, spinel, plagioclase, merrillite (whitlockite), kamacite, and troilite (Fig. 1). The appearance is similar to terrestrial cumulus harzburgite except for the presence of metallic iron.

The abundance obtained by the CMA map is shown in Table 1 with those by

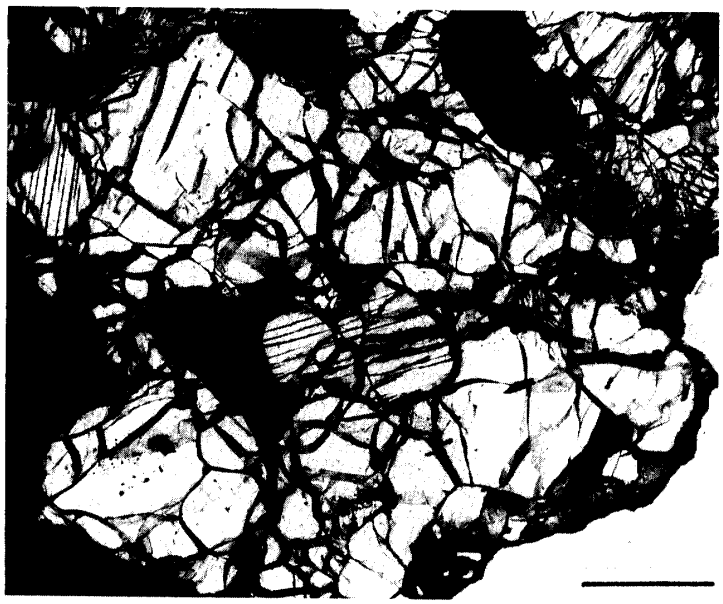

Fig. 1. Photomicrograph showing the coarse-grained texture of Y-791493. Transmitted light. Scale bar represents 1 mm.

Table 1. Bulk chemical composition and modal composition of Y-791493.

	Bulk*	Mode	(1)	(2)	(3)
	(wt %)		(%)		
SiO_2	34.90	Olivine	39.9	41.8	43.1
TiO_2	0.05	Orthopyroxene	33.9	38.8	37.2
Al_2O_3	0.90	Clinopyroxene	3.3		tr
FeO	6.12	Spinel	5.7	3.1	1.0
Fe_2O_3	6.02	Plagioclase	6.2	1.3	1.6
MnO	0.42	Merrillite	0.3	3.7	5.0
MgO	29.53	Fe-Ni metal	7.0	9.8	9.1**
CaO	1.54	Troilite	3.7***	1.5	3.0
Na_2O	0.21				
K_2O	<0.02				
Cr_2O_3	0.81				
P_2O_5	0.49				
Fe	14.28				
Ni	1.13				
Co	0.07				
FeS	2.10				
$H_2O(+)$	1.1				
$H_2O(-)$	0.04				
Total	99.7				
Fe_{tot}	31.2				

(1): This study. (2): YANAI and KOJIMA (1982). (3): YANAI *et al.* (1984).
*: HARAMURA *et al.* (1983). **: Kamacite and schreibersite. ***: Appears to contain oxidized iron.

YANAI and KOJIMA (1982) and YANAI *et al.* (1984). The results show noticeable differences suggesting the presence of heterogeneity among the samples; the amounts of clinopyroxene, plagioclase, merrillite, and troilite are especially variable. These phases, as will be discussed below, crystallized after olivine and orthopyroxene filling

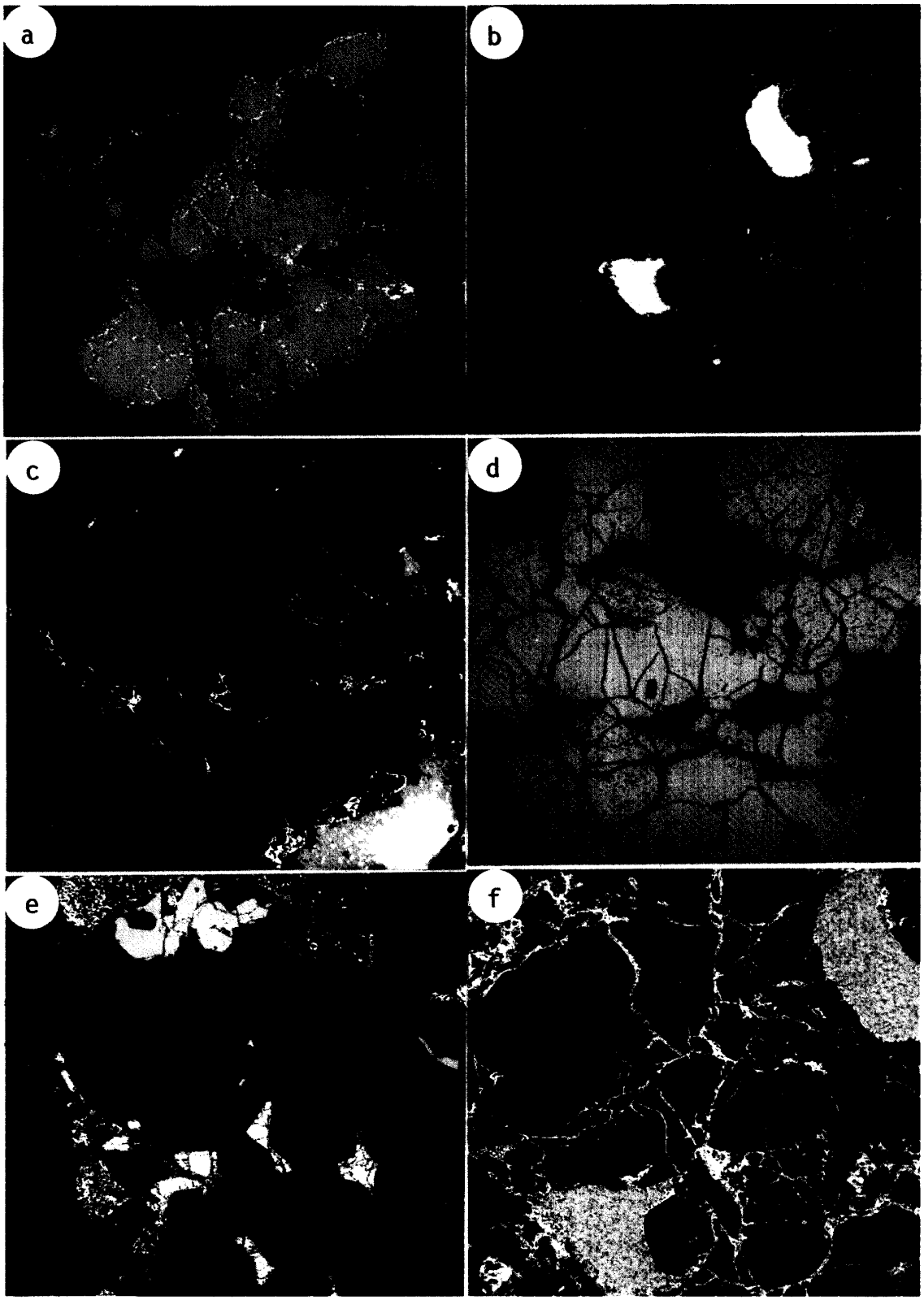

Fig. 2. CMA photographs of Y-791493.

the interstitial space of euhedral to subhedral olivine and orthopyroxene. This suggests that residual melt was distributed heterogeneously among previously crystallized phases.

Figure 2a shows the distribution of Mg where olivine, orthopyroxene, clinopyroxene, spinel, and other phases can be distinguished by different colors. As shown in the figure, olivine (pink) and orthopyroxene (red) show euhedral to subhedral shapes, mostly several hundred μm to 1 mm in size (see Fig. 4). The edges of large grains are generally rounded. A large, subhedral spinel grain (blue) occurs in the upper right, and small spinel occurs within olivine or along grain boundaries. Spinel is commonly associated with troilite. Clinopyroxene (green) is anhedral occurring interstitially between orthopyroxene and/or olivine grains; and some clinopyroxenes exist as exsolution lamellae in orthopyroxene. Figure 2b shows the distribution of Fe, where kamacite (white) and troilite (pink) are well recognized. Figure 2c shows the distribution of Na showing systematic distribution of anhedral plagioclase. Two layers of plagioclase grains form alignments in the direction of ENE-WSW of the figure. The distribution of olivine and orthopyroxene grains shows a weak preferred orientation (foliation) parallel to the plagioclase-rich bands. The large olivine grains tend to lie with their (001) surface parallel to the bands. Troilite is commonly associated with metal and is abundant in a plagioclase-rich band (Fig. 2b). Conversely, Fe-Ni metal, clinopyroxene, and large spinel grains are elongated perpendicular to these bands. Most of metal grains occur in the plagioclase-rich bands. The presence of the bands is suggestive of layering.

4. Petrofabric

In order to clarify the relationship between the plagioclase-rich bands and the olivine fabric, we have conducted a petrofabric analysis of olivine grains. Results

a. *Distribution of Mg. Pink: MgO>35wt% (olivine), red: 35–28% (orthopyroxene), green: 22–14% (clinopyroxene), dark blue: 8–3% (spinel), black: 3–0% (Fe-Ni metal, troilite, plagioclase, and merrillite). Large euhedral to subhedral olivine and orthopyroxene are visible. Olivine inclusions in orthopyroxene are well shown.*

b. *Distribution of Fe. White: Fe>90wt% (Fe-Ni metal), pink: Fe>60wt% (troilite and oxidized iron), red: FeO 24–19wt% (spinel), green: 15–10% (olivine), light blue: 10–5% (orthopyroxene), dark blue: 5–2% (clinopyroxene). Metal and troilite can be distinguished.*

c. *Distribution of Na. Red: 11–6wt% (plagioclase), light blue: 3–1% (merrillite), dark blue: 1–0.4% (clinopyroxene). Yellow to light blue in the lower right is a glass mount. Plagioclase defines banded structure.*

d. *Distribution of Mg/Fe ratio in a part of Y-791493. White: >15 (merrillite, in the upper right corner neighbouring spinel), red: 12–9, yellow: 9–5 (olivine and orthopyroxene), dark blue: 2–0.7 (spinel). Orthopyroxene has a little higher Mg/Fe than olivine and is shown as yellow with red dots. Strong Mg-Fe zoning in olivine is locally present toward spinel, metal, and troilite.*

e. *Distribution of Ca/(Ca+Mg+Fe) ratio in a part of Y-791493. White: 1.0 (plagioclase), yellow 0.5–0.35 (clinopyroxene), light blue: 0.1–0.025 (orthopyroxene), dark blue: 0.025–0.01 (orthopyroxene). Ca-rich core of orthopyroxene is clearly shown.*

f. *Distribution of Fe/Ni. Green: 0.1–0.05 (kamacite), Green and light blue streaks indicate that Ni was dissolved from Fe-Ni metal and precipitated along grain boundaries or cracks in silicates.*

show that the fabric is characterized by a strong maximum of $Y(c)$ axes normal to the plane of thin section (Fig. 3). This indicates that the thin section was cut almost perpendicular to the olivine lineation. Orientation of $X(b)$ axes is relatively random, but they show a weak concentration almost perpendicular to the Y maximum and plagioclase-rich bands. This concentration corresponds to the visible foliation parallel to the plagioclase-rich bands. $Z(a)$ axes do not show a strong concentration either, but display a girdle nearly parallel to the thin section plane (normal to Y maximum) (Fig. 3). A weak concentration of Z axes is recognizable, indicating that the Z axes tend to lie parallel to the plagioclase-rich bands. Orthopyroxene shows a fabric similar to that of olivine, although available grains of orthopyroxene are restricted and the results are less clear. The fabric of orthopyroxene is characterized by maximum of $Z(c)$ axes normal to the thin section plane, a weak concentration of $X(b)$ axes close to that of the $Z(a)$ axes of olivine, and a minor concentration of $Y(a)$ axes vertical to the X and Z axes. From the presence of plagioclase-, metal-, and troilite-rich bands and a strong concentration of Y axes of olivine perpendicular to the thin section plane, it is suggested that plagioclase-rich *layers* do exist and that they probably lie parallel to the olivine lineation.

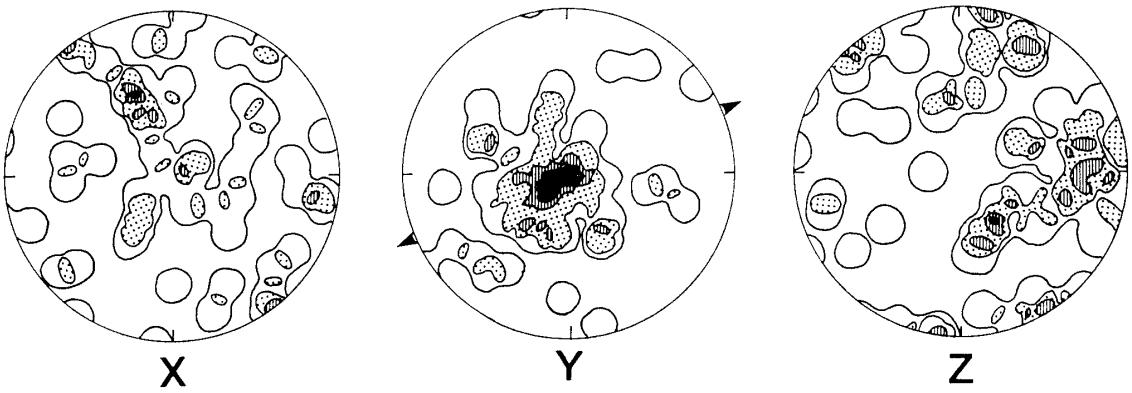

Fig. 3. Equal-area, lower hemisphere projection of olivine indicatrix axes. Arrowheads on the primitive indicate direction of plagioclase-rich bands. Contours: 2, 4, 6, 8, and 10% per 1% area. Measurements on 50 grains.

Y concentrations of olivine were reported from terrestrial rocks: olivine phenocrysts in basalt (BROTHERS, 1959); banded troctolite (HUANG and MERRITT, 1952); dunite (YOSHINO, 1961). Y concentrations in the former two cases are the results of magmatic flow, in which the long Y axes are aligned parallel to the linear element in the flow plane indicating the direction of movement. In magmatic flow, the flat X axes show a maximum parallel to the boundary surface of the laminar flow, and thus vertical to the Y concentration.

Y concentration is also found in meteorites (Dingo Pup Donga ureilite: BERKLEY *et al.*, 1980; ALH-77005: BERKLEY and KEIL, 1981). BERKLEY and KEIL (1981) concluded that the olivine fabric in ALH-77005 may have been formed by flow of melt rather than accumulation of olivine crystals on the stagnant floor of a cumulate reservoir. The strong preferred orientation of direction of c axes of olivine and orthopyroxene in the layering plane in Y-791493 indicates the existence of a strong magmatic

laminar flow parallel to the direction of their elongation at the time of formation. Plagioclase-rich layers parallel to the lineation and weak foliation of olivine may correspond to melt-rich layers in the laminar flow.

5. Mineralogy

5.1. *Olivine*

The cores of olivine are homogeneous throughout the sample, the Fo content being 87 to 88. Representative chemical compositions are shown in Table 2. The olivines contain considerable amounts of MnO (about 0.5–0.6 wt%) and undetectable CaO and NiO. Some olivine grains are homogeneous and show no detectable zoning. Some, however, show a noticeable compositional zoning; the rim is more enriched in Mg than the core. The rim composition of such grains ranges from Fo_{88} to Fo_{91}.

Mg enrichment toward spinel is conspicuous, which is well shown in the CMA map of Mg/Fe (Fig. 2d). Figure 4 shows the Mg/(Mg+Fe) ($=X_{Mg}$) zoning profile

Table 2. Chemical composition of olivine, orthopyroxene, and clinopyroxene.

	Ol (1)	Ol (2)	Ol (3)	Opx (1)	Opx (2)	Cpx (1)	Cpx (2)
(wt %)							
SiO_2	39.7	40.1	39.7	55.8	56.5	54.5	54.1
TiO_2	0	0	0	0.14	0.23	0.31	0.38
Al_2O_3	0.08	0	0	0.29	0.49	0.60	0.92
FeO	12.0	8.89	12.7	8.69	7.78	2.97	3.35
MnO	0.58	0.54	0.54	0.56	0.57	0.23	0.34
MgO	46.7	49.3	46.6	32.7	31.8	17.4	17.6
CaO	0	0	0	0.75	1.57	22.4	20.7
Na_2O	0	0	0	0.03	0.04	0.55	0.67
Cr_2O_3	0	0.31	0	0.20	0.47	0.95	1.38
Total	99.1	99.1	99.5	99.2	99.5	99.9	99.4
(Cation)	O=4			O=6		O=6	
Si	0.995	0.991	0.993	1.971	1.984	1.985	1.977
Ti	0	0	0	0.004	0.006	0.008	0.010
Al	0.002	0	0	0.012	0.020	0.026	0.040
Fe	0.251	0.184	0.266	0.257	0.228	0.090	0.102
Mn	0.012	0.011	0.011	0.017	0.017	0.007	0.010
Mg	1.744	1.815	1.737	1.722	1.665	0.943	0.959
Ca	0	0	0	0.028	0.059	0.874	0.811
Na	0	0	0	0.002	0.003	0.039	0.048
Cr	0	0.006	0	0.006	0.013	0.028	0.040
Sum	3.004	3.007	3.007	4.019	3.995	4.000	3.997
Mg/(Mg+Fe)	0.874	0.908	0.867	0.881	0.879	0.913	0.910
En				87.0	85.3	49.4	51.7
Fs				11.7	11.7	4.8	5.1
Wo				1.3	3.0	45.8	43.2

Ol (1): Representative composition of olivine, Ol (2): most magnesian olivine in the rim contacting with spinel, Ol (3): most ferrous olivine in the core, Opx (1): most Wo-poor opx in the rim, Opx (2): most Wo-rich opx in the core. Cpx (1): most Wo-rich cpx in the rim, Cpx (2): most Wo-poor cpx in the core.

across an olivine and a large spinel: Olivine becomes magnesian from the core to boundary with spinel; in contrast, X_{Mg} of spinel decreases toward the boundary. Similar zoning patterns are observed in olivine grains containing small spinel inclusions. Olivine becomes highly magnesian toward the spinel inclusions and also toward the outer margins of the crystals. As discussed below, the Mg-Fe zoning in olivine and spinel is considered to have been formed by cation exchange during cooling and not by reduction.

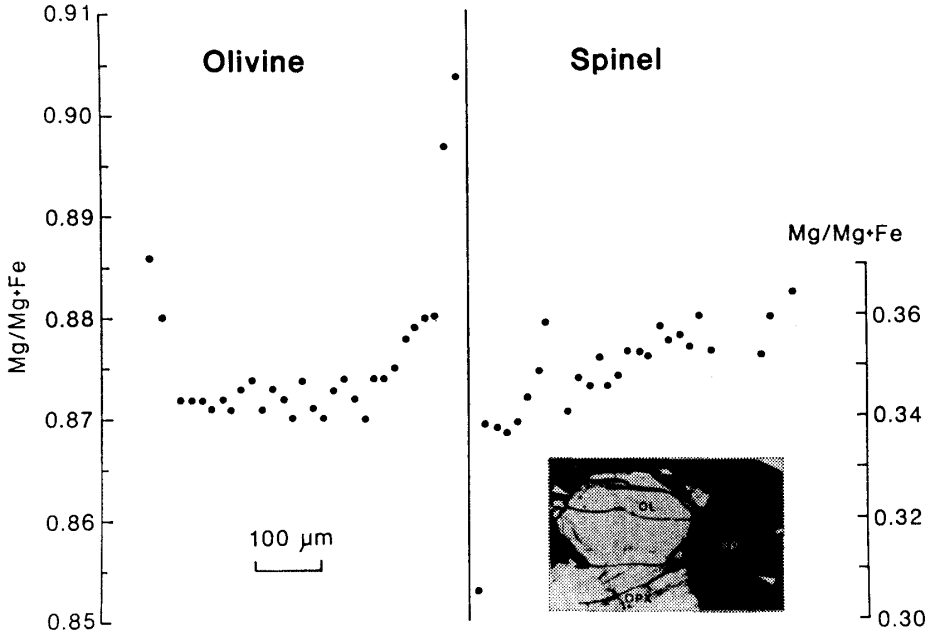

Fig. 4. Mg/(Mg+Fe) zoning profile crossing olivine and large spinel grain boundary. Olivine shows strong Mg-enrichment pattern and spinel shows Mg-depletion pattern toward the grain boundary. The position of profile is shown in the photomicrograph by two arrow-heads. Abbreviations are; ol: olivine, opx: orthopyroxene, sp: spinel.

Olivine often shows Mg enrichment toward the rim without contiguous spinel. In such cases, the neighboring phases are either Fe-Ni metal, troilite, orthopyroxene, or albite. Some olivines become Mg-rich toward one of these phases but some do not. NAGAHARA and OZAWA (1985) considered that the Mg-Fe zoning without adjacent spinel had been formed by reduction of olivine by an unknown reducing agent, possibly carbon, after solidification. If carbon was heterogeneously distributed, it might have acted as a reducing agent to cause the reduction of neighboring olivine. Alternatively, Mg-rich rims could be formed by cation exchange between olivine and spinel during cooling if large spinels exist as an adjacent phase in the third dimension of the sample.

Olivine also occurs as small (up to 20 μm) inclusions in orthopyroxene. In Fig. 2a, rounded inclusions of olivine (pink) are well shown in orthopyroxene host (red). These olivines are Fo_{87}, the same as that of homogeneous cores of the large euhedral grains.

Olivine often contains fine spherical inclusions in bead-like arrays; the spherules are Fe-Ni metal, troilite, and/or rarely spinel. Similar occurrences have been reported

in olivine in pallasites and ureilites (BUSECK, 1977; BERKLEY *et al.*, 1980).

5.2. *Orthopyroxene*

Cores of orthopyroxene are roughly homogeneous among grains in thin sections studied, X_{Mg} being about 0.88. Representative compositions are shown in Table 2. They contain small amounts of Al_2O_3 (0.3–0.5 wt%), TiO_2 (0.1–0.2%), Cr_2O_3 (0.2–0.5%), and MnO (0.5–0.6%).

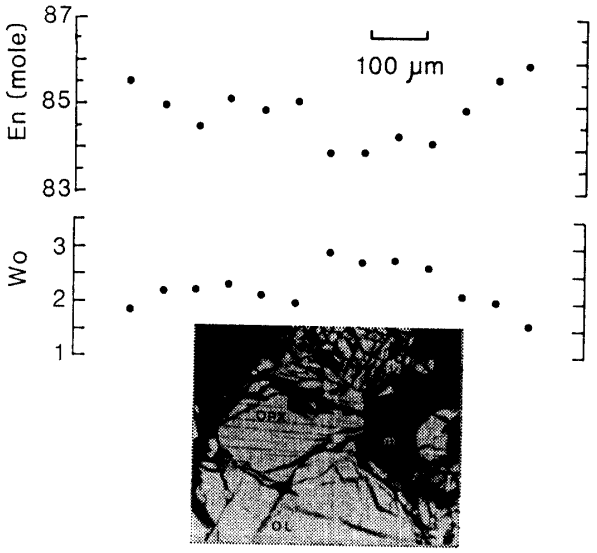

Fig. 5. Wo and En zoning profile of orthopyroxene grain coexisting with kamacite and olivine. Profile is symmetrical regardless of adjacent phases. The position of the profile is shown in the photomicrography by two arrowheads. Abbreviations are; m: metal, ol: olivine, opx: orthopyroxene.

Each grain shows a weak compositional zoning where the En mole% increases and the Wo mole% decreases outward regardless of neighboring phases. Figure 2e shows the distribution of Ca/(Ca+Mg+Fe) in orthopyroxene, which reveals depletion of CaO toward the margin and the presence of numerous exsolution lamellae in the central portion of the grain. The maximum range is $En_{85}Wo_3$ at the core to $En_{87}Wo_{1.3}$ at the rim (Table 2). Figure 5 shows the zonal pattern of En and Wo in orthopyroxene neighboring Fe-Ni metal and olivine; En increases, but Wo decreases continuously outward from the grain core. Around olivine, pyroxene shows a slight En increase and Wo decrease toward an olivine inclusion (Fig. 2e). Compositional zoning in orthopyroxene is considered to have been formed by cation diffusion between clinopyroxene and exsolution of clinopyroxene at the core of orthopyroxene during cooling as usually observed in slowly cooled terrestrial, lunar, and achondritic rocks.

Orthopyroxene is rarely included in olivine. It is present, if at all, in the outer portion of olivine grains; the composition of these inclusions is similar to the rims of large, euhedral orthopyroxene grains.

5.3. *Clinopyroxene*

As mentioned earlier, clinopyroxene is anhedral, and is easily recognized in the

CMA map of MgO (Fig. 2a, green). Representative chemical compositions are shown in Table 2. They contain small amounts of Al_2O_3 (0.6 wt%), TiO_2 (0.3%), less MnO (0.3%) than orthopyroxene, and considerable amounts of Cr_2O_3 (1.0 wt%).

Clinopyroxene, as well as orthopyroxene, shows compositional zoning, En mole decreases and Wo mole increases from the center to the margin, ranging from $En_{52}Wo_{41}$ in the core to $En_{49}Wo_{46}$ at the rim (Table 2). This zoning pattern is considered to have been formed by cation diffusion between clinopyroxene and orthopyroxene during cooling.

Clinopyroxene occurs also as exsolution lamellae in the core of orthopyroxene; they appear in Fig. 2e as ambiguous streaks. Lamellar clinopyroxene are identical in composition to the large anhedral grains.

5.4. *Spinel*

Spinel occurs mostly as small inclusions in olivine or as small grains along grain boundaries, often associated with troilite. Representative chemical compositions of spinels are shown in Table 3. They are chromite (59–66 wt% Cr_2O_3, 4–8% Al_2O_3) with considerable amounts of TiO_2 (0.2–1.2 wt%), V_2O_3 (0.5–0.8%), MnO (1.0–1.6%), and ZnO (0.7–1.8%); spinel with high ZnO content is also the case for other related meteorites (Lodran, Acapulco, "primitive achondrites", "winonaites", "forsterite chondrites", silicate inclusions in IAB and IIICD irons) (BILD and WASSON, 1976; BILD, 1977; GRAHAM *et al.*, 1977; TAKEDA, *et al.*, 1980; PALME *et al.*, 1981; PRINZ

Table 3. Chemical composition of spinel.

	(1)	(2)	(3)	(4)	(5)
(wt %)					
Al_2O_3	5.98	7.55	7.47	7.81	4.03
TiO_2	0.66	1.11	1.10	0.93	0.19
FeO	23.9	21.6	22.3	24.1	25.0
MnO	1.36	1.07	1.22	1.32	1.04
MgO	4.82	7.00	6.16	4.84	3.61
Cr_2O_3	61.9	62.0	60.9	59.8	63.7
V_2O_3	0.66	0.56	0.54	0.82	0.55
ZnO	0.80	0.54	0.60	0.78	1.39
Total	100.1	101.4	100.3	100.4	99.5
(Cation)	O=4				
Al	0.246	0.299	0.301	0.317	0.170
Ti	0.017	0.028	0.028	0.024	0.005
Fe	0.697	0.607	0.637	0.694	0.748
Mn	0.040	0.031	0.035	0.039	0.032
Mg	0.251	0.351	0.314	0.248	0.193
Cr	1.707	1.647	1.646	1.628	1.802
V	0.019	0.015	0.015	0.023	0.016
Zn	0.021	0.013	0.015	0.020	0.037
Sum	2.997	2.991	2.991	2.992	3.001
Mg/(Mg+Fe)	0.264	0.366	0.330	0.264	0.205
Cr/(Cr+Al)	0.874	0.846	0.845	0.837	0.914

(1): Average of 20 analyses, (2): Core of large euhedral spinel (577 μm in size), (3): Rim of large spinel (1), (4): Medium-grained (35 μm) spinel in grain boundary, (5): Small grain (8.8 μm) in olivine.

et al., 1980, 1983). As discussed above (Fig. 4), large grains show a feeble compositional zoning in Mg and Fe. Medium-grained spinel, which is always present along grain boundaries, shows Al- and Fe-enrichment and Mg- and Cr-depletion toward the rim. The smallest spinel grains exist in the interior of olivines and are sometimes associated with troilite.

There is a relationship between the composition and the grain size of spinel. With increasing grain size, Al_2O_3, MgO, and TiO_2 increase (Fig. 6), and Cr_2O_3, FeO, and ZnO decrease. V_2O_3 does not show a clear relationship. The MnO content generally increases as the grain size decreases with the exception of two grains, which are small inclusions in olivine with no associated phase (*e.g.*, troilite or metal). These two grains are anomalously poor in MnO (1.0 wt%). This relationship between grain size and composition may be due to the difference in the stage of crystallization of spinel. Though Mg, Fe, and probably Mn were exchanged among olivine, pyroxenes, and spinel during cooling, trivalent elements, Al, Cr, and Ti, remain constant in spinel below the solidus temperature and are good indicators of the chemical composition of the silicate melt during spinel crystallization. In the case of terrestrial peridotites

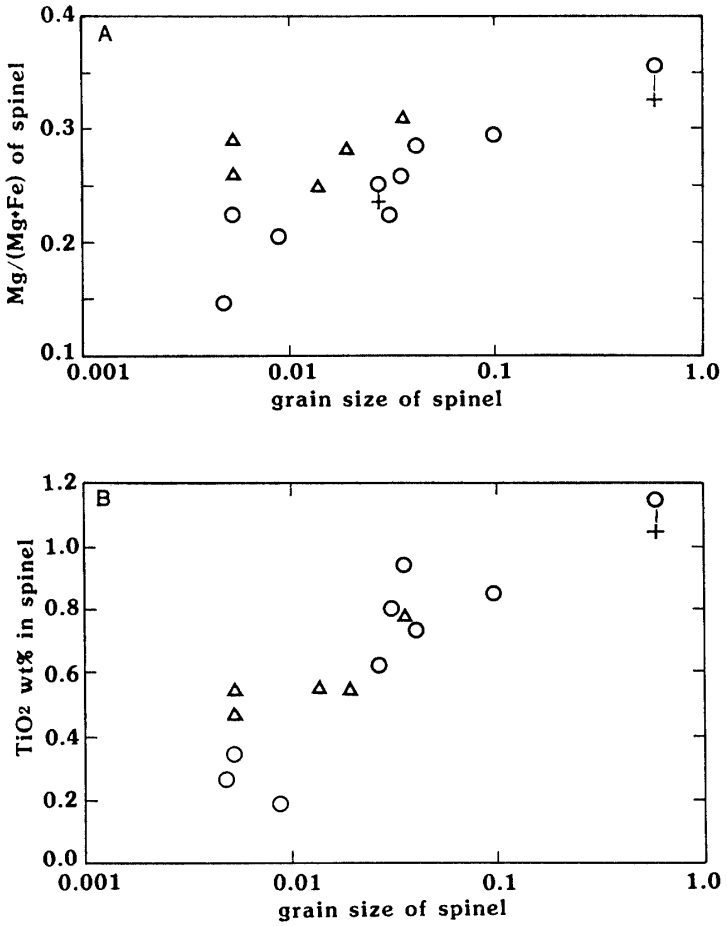

Fig. 6. Relationships between Mg/(Mg+Fe) ratio (A) and TiO_2 content (B) of spinel and its grain size. Symbols; open circle: core of spinel in contact with or included in relatively homogeneous olivine, open triangle: core of spinel in contact with or included in anomalously Mg-rich olivine, plus: rim of spinel.

from the upper mantle, spinel which crystallizes from a silicate melt in the early stage of crystallization is rich in Cr, and tends to become enriched in Al as temperature decreases (DICK and BULLEN, 1984). Therefore, small, Cr-rich spinel embedded in olivine was probably the earliest phase, being trapped in the crystallizing olivine at the highest temperature (at the stage of maximum degree of melting). Only small grains could be trapped in olivine and relatively large grains could not be trapped. With the decrease of temperature, spinel becomes richer in Al and Ti because the silicate melt becomes enriched in these elements. The largest spinels continue to maintain equilibrium with the silicate melt until the end of spinel crystallization and are richest in Al and Ti and depleted in Cr.

5.5. *Other phases*

Plagioclase occurs as an interstitial film (Fig. 2c) and is partly twinned. Chemical composition is roughly homogeneous among grains ranging from $An_{18}Ab_{80}Or_2$ to $An_{20}Ab_{77}Or_3$, which is more sodic and less potassic than plagioclase in other related meteorites ($An_{34}Ab_{62}Or_4$ in Acapulco and ALH-77081). It shows a slight but systematic compositional zoning; K and Ca increase and Na decreases from the center to the margin. Representative composition is shown in Table 4.

Only one merrillite grain exists in our thin section and is well shown in the CMA

Table 4. Representative chemical composition of plagioclase and merrillite.

	Plagioclase		Merrillite	
(wt %)				
SiO_2	64.9	65.2	n.d.	n.d.
TiO_2	0	0	—	—
Al_2O_3	22.7	22.5	n.d.	n.d.
FeO	0.09	0.23	0.23	0.28
MgO	0	0	3.56	3.54
CaO	4.05	3.74	45.3	45.1
Na_2O	9.31	9.29	2.65	2.53
K_2O	0.47	0.57	n.d.	n.d.
P_2O_5	n.d.	n.d.	47.3	47.4
Total	101.5	101.5	99.0	98.9
(Cation)	O=8		O=56	
Si	2.827	2.839	—	—
Ti	0	0	—	—
Al	1.165	0.155	—	—
Fe	0.003	0.008	0.069	0.082
Mg	0	0	1.890	1.882
Ca	0.189	0.175	17.308	17.232
Na	0.786	0.784	1.832	1.753
K	0.026	0.032	—	—
P	—	—	14.286	14.338
Sum	4.996	4.993	35.385	35.287
An	18.9	17.7		
Ab	78.5	79.1		
Or	2.6	3.2		

n.d.: not determined.

map of Na (Fig. 2c, light blue). Merrillite is interstitial and its occurrence is very similar to that of plagioclase, indicative of crystallization from an interstitial melt. It contains about 2 wt% Na_2O and 3.5% MgO (Table 4). YANAI *et al.* (1984) reported the presence of chlorapatite along with merrillite in another thin section of Y-791493.

Fe-Ni metal occurs as large anhedral grains, and is homogeneous throughout the thin sections studied. As shown in Fig. 2f, the Fe/Ni ratio is constant between and among grains indicating that all metal grains are homogeneous kamacite. The Ni content ranges from 6.5 to 6.8 wt% (Table 5), and the P and Co contents are about 0.1 and 0.5 wt%, respectively (Table 5). Fe-Ni metal occurs also as tiny spherical inclusions in olivine or orthopyroxene; the chemical composition of these spherules varies from grain to grain, with Ni content ranging from almost 0 to about 7%. YANAI *et al.* (1984) reported schreibersite in another thin section of Y-791493.

Troilite occurs as small subhedral grains in grain boundaries coexisting with either Fe-Ni metal or spinel. It is almost pure FeS with a small amount of Cr (0.1–0.22 wt%) (Table 5), but troilite inclusions in olivine contain up to 1.0 wt% Cr.

6. Discussion

6.1. *Crystallization of Y-791493*

The crystallization sequence of constituent minerals can be estimated from the

Table 5. Representative chemical composition of kamacite and troilite.

	Kamacite		Troilite		
	(1)	(2)	(1)	(2)	(3)
(wt %)					
Fe	92.5	92.4	63.3	63.1	62.5
Ni	6.88	6.94	0	0	0
Co	0.49	0.49	0	0	0
Cr	0	0	0.12	0.22	1.09
P	0.12	0.11	0	0	0
S	0	0	36.7	36.2	35.8
Si	0	0	0	0	0
Ti	0	0	0	0	0
Mn	0	0	0	0	0
Zn	0	0	0	0	0
Total	100.0	100.0	100.1	99.5	99.4
(mol %)					
Fe	0.928	0.927	0.497	0.500	0.496
Ni	0.066	0.066	0	0	0
Co	0.004	0.005	0	0	0
Cr	0	0	0.001	0.002	0.009
P	0.002	0.002	0	0	0
S	0	0	0.502	0.498	0.495
Ti	0	0	0	0	0
Mn	0	0	0	0	0
Zn	0	0	0	0	0
Sum	1.000	1.000	1.000	1.000	1.000

Kamacite (1) and (2) and Troilite (1) and (2): representative composition, Troilite (3): Most Cr-rich troilite occurring as a small inclusion in olivine.

texture and occurrence. Small spinel inclusions in olivines indicate that spinel crystallized first followed by olivine. Olivine is often enclosed in orthopyroxene and orthopyroxene is rarely enclosed in olivine indicating the simultaneous crystallization of these two phases at a certain stage of crystallization. The lack of pigeonite and the presence of orthopyroxene in Y-791493 suggest that the maximum equilibrium temperature during crystallization was below about 1200°C. As shown later, the crystallization temperature of pyroxenes was higher than 1100°C, thus, the equilibrium temperature at the last stage of melting was between 1200 and 1100°C.

During the crystallization of olivine and orthopyroxene, silicate melt and metal-sulfide melt existed as interstitial melts. This is shown by the presence of tiny blebs and irregular inclusions inside olivine and orthopyroxene. The tiny blebs are mostly Fe-Ni metal and troilite. Troilite sometimes coexists with merrillite, forming ovoid inclusions (Fig. 7a), which shows that two melts were simultaneously trapped into olivine. The blebs occasionally form alignments along crystallographic directions (Fig. 7b), and are distributed on (021) and rarely (010) planes of olivine. These are characteristic crystals faces of olivine, supporting the possibility of a trapped melt origin for these blebs. Blebs of Fe-Ni metal and/or troilite sometimes rim the olivine inclusions in orthopyroxene (Fig. 7c).

Clinopyroxene and Fe-Ni metal crystallized after olivine and orthopyroxene. They are coarse-grained, similar in size to olivine and orthopyroxene, but are anhedral indicating that they crystallized from an interstitial melt. Plagioclase and merrillite are the last phases to have crystallized in the interstices which remained nearly perpendicular to the early crystallized olivine and orthopyroxene grains.

6.2. Cooling history

Several kinds of information on the thermal history of Y-791493 can be obtained by using different mineral assemblages. The highest temperature record is estimated from coexisting ortho- and clinopyroxenes. Ca depletion from core to rim of orthopyroxene and Ca increase from core to rim of clinopyroxene are evidently the results of cation diffusion during cooling. Using the full compositional difference between the two pyroxenes, $En_{85}Wo_{3.0}$ and $En_{86}Wo_{1.4}$ for the core and the rim of orthopyroxene, respectively, and $En_{49.4}Wo_{45.8}$ and $En_{51.2}Wo_{43.3}$ for those of clinopyroxene (Table 2), we get temperatures of 1100 to 800°C for orthopyroxene and 1120 to 1020°C for clinopyroxene by using the two-pyroxene thermometer recently revised by LINDSLEY and ANDERSEN (1983) (Fig. 8). As pyroxenes contain little Al_2O_3, the error of these temperatures should be small.

Information at lower temperatures is obtained by olivine and spinel. OZAWA (1983) found in terrestrial peridotites that the composition of spinel enclosed in homogeneous olivine strongly depends on the size of spinel and that this is due to diffusion-controlled subsolidus Mg-Fe exchange. X_{Mg} of cores of spinels in Y-791493 decreases remarkably with decreasing grain size of spinel, and is probably due to the same mechanism as that in the terrestrial peridotites. OZAWA (1984) has developed a "geospeedometer" on the basis of the dependence of spinel composition on its grain size. Application of olivine-spinel geospeedometry to Y-791493 is shown in Fig. 9. It is necessary to use the composition of spinel embedded in the homogeneous portion of

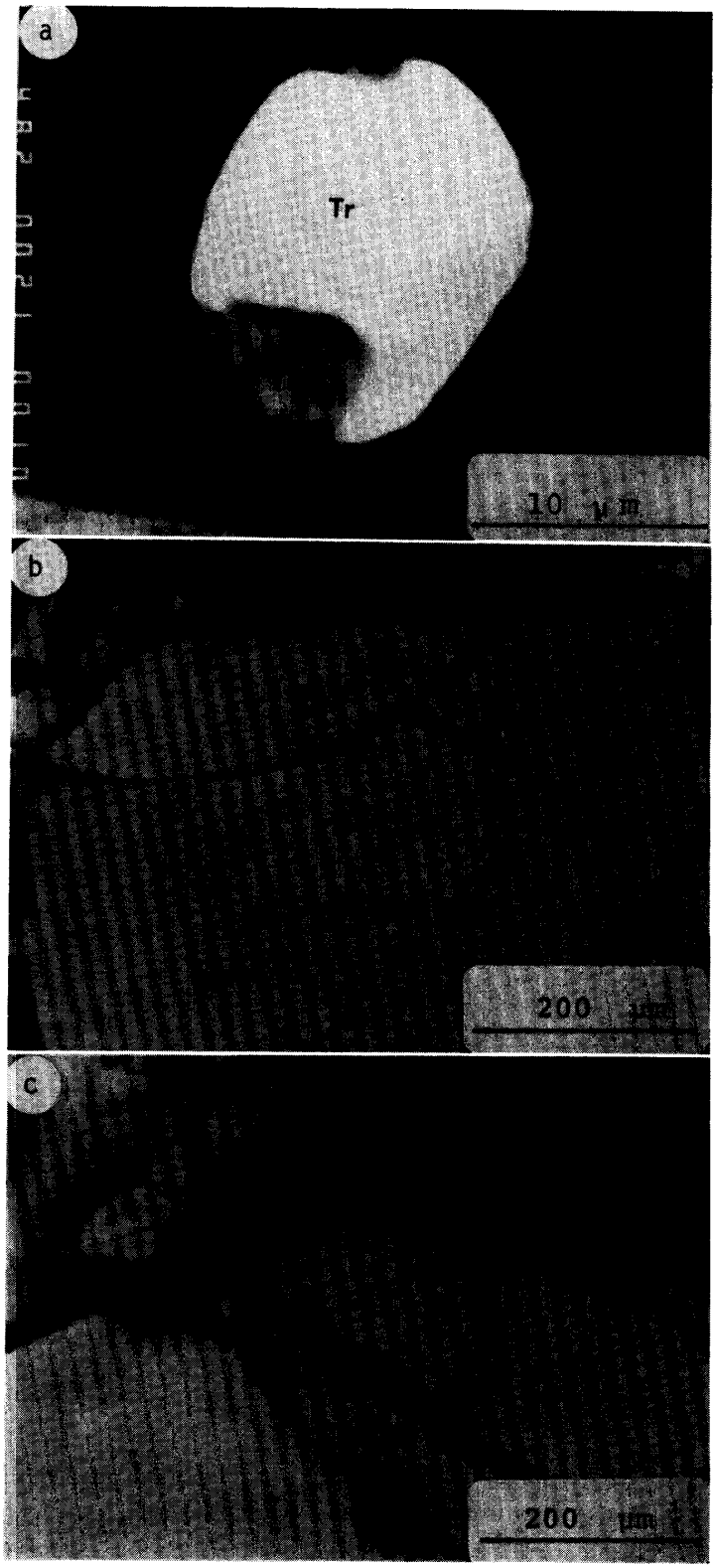

Fig. 7. Occurrence of small globules of metal and troilite. Abbreviations are; tr: troilite, mer: merrillite, ol: olivine, op: orthopyroxene.

a. Back-scattered electron image of merrillite and troilite composite inclusion in olivine.

b. Metal and troilite inclusion in olivine. The inclusions are arranged to form a ring. Transmitted light.

c. Metal and troilite present between olivine inclusions and its host orthopyroxene. Transmitted light.

olivine grains. Spinel in the strongly zoned rim of olivine will not give a correct value; these are shown as a different symbol in Fig. 9 and were excluded for the calculation of geospeedometry. Difference of contents of trivalent elements will not largely

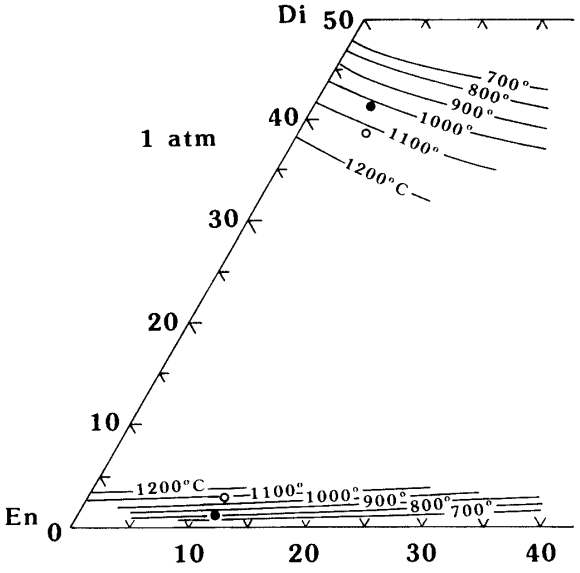

Fig. 8. Composition of coexisting orthopyroxene clinopyroxene plotted onto part of the pyroxene thermometer of LINDSLEY *and* ANDERSEN *(1983). Mole fraction of Wo, En, and Fs were obtained according to the projection scheme of* LINDSLEY *and* ANDERSEN *(1983). Symbols are; open circle: core, closed circle: rim.*

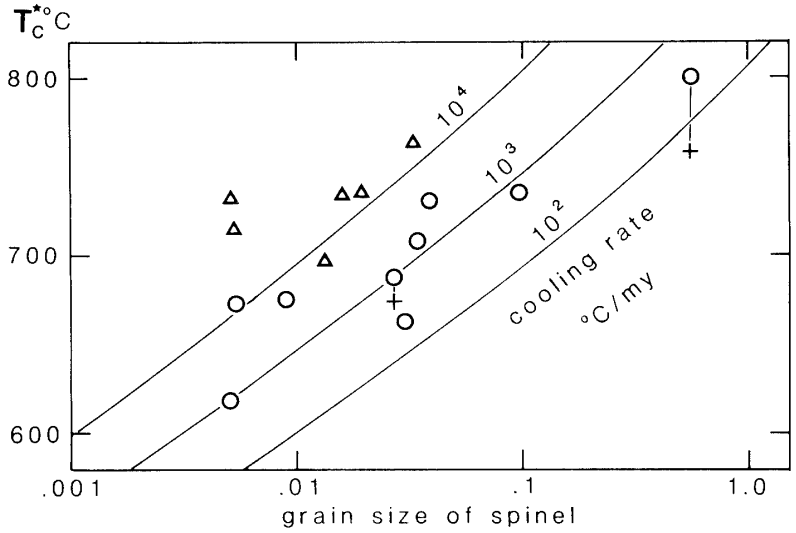

Fig. 9. Relation between grain size of spinel and temperature calculated by pairing the core of olivine and spinel (T_c). T_c* was calculated using the average core composition of olivine including or neighboring spinel. The symbols are the same as those in Fig. 6. Triangles were not used for geospeedometry. Diffusion data used to calculate the constant cooling rate curves are: $Q_{ol}=3.45$ (eV), $Q_{sp}=3.6$, $D_{0,ol}=3.0$ (cm^2/s), $D_{0,sp}=5.0$. These values are for spinel with $Cr/(Cr+Al)$ 0.8. The constant coolingrate curves for Y-791493 ($Cr/(Cr+Al)=0.82$–0.91) may slightly shift to high T_c*.*

affect the result. Though the grain size variation is not wide and the number of available grains is not large, an approximate cooling rate of 10^3 °C/Ma is obtained in the temperature range of 800 to 600°C. If we take the effect of high Cr content in spinel into account, the cooling rate may be a little larger.

All Fe-Ni metal grains in the thin sections studied are kamacite alone, neither taenite nor schreibersite was found by us, although YANAI *et al.* (1984) reported schreibersite composition. The lack of these phases makes it impossible to estimate the

metallographic cooling rate at low temperatures. BILD and WASSON (1976) estimated the metallographic cooling rate of Lodran for 700°C/Ma at high temperatures and 30°C/Ma for low temperatures using the size and composition of taenite. PRINZ *et al.* (1978), using the relationship between size and composition of zoned schreibersite lamellae in kamacite, obtained a cooling rate of about 10°C/Ma for Lodran. If we use the recently revised diffusion coefficient of NARAYAN and GOLDSTEIN (1985), these cooling rates must be revised to be larger by two orders of magnitude. As the composition of schreibersite in Y-791493 (YANAI *et al.*, 1984) is close to that of Lodran, and in spite of the fact that the width of the schreibersite lamellae is not known, we can roughly say that the metallographic cooling rate of Y-791493 could be close to that of Lodran. The metallographic cooling rate of 10^3 °C/Ma at 500°C agrees well with that estimated from olivine-spinel geospeedometry. Therefore, it is concluded that Y-791493 cooled continuously from above 1100°C to below 500°C without any thermal interruption or reheating.

6.3. *Formation of Y-791493*

HARAMURA *et al.* (1983) made a wet chemical analysis of Y-791493 and showed that it is severely weathered. It contains 6.02 wt% Fe_2O_3, which is probably present as Fe hydroxide surrounding Ni-Fe metal or troilite. It also occurs as reddish brown, thin veins in olivine or along grain boundaries of silicates. The mode of occurrence of Fe_2O_3-rich phases indicates that Fe_2O_3 was mainly derived from Fe-Ni metal and partly from troilite. This alteration of metallic iron and troilite into Fe_2O_3-rich phases with loss of Ni, Co, and S might lower the contents of these elements in the bulk composition. In the following discussion, all Fe_2O_3 is assumed to be derived from metallic iron, because the bulk FeO/MgO ratio given by HARAMURA *et al.* (1983) is consistent with the X_{Mg} of olivine and orthopyroxene. Based on this assumption, the bulk chemical composition of Y-791493 with that of the average Antarctic H-chondrite is given in Table 6 with their silicate portions recalculated to 100%. Table 6 also compares these compositions with those of Lodran, Acapulco, and ALH-77081 meteorites.

As the bulk chemical composition of Y-791493 is roughly chondritic, it is valid to consider the precursor material of Y-791493 to be a kind of chondrite or a mixture of some of them. Figure 10 shows the relationship between amount of Fe in oxides and Fe in metal and sulfide (Urey-Creig diagram) of Y-791493 as compared with ordinary chondrites, which is a good indicator of redox state and of bulk iron content of meteorites. Y-791493 falls within the variation of H-chondrites, though relatively biased to the reducing portion. The precursor could be similar to H-chondrites in major chemistry but it melted and solidified in more reducing conditions than the average H-chondrite.

Although Y-791493 and H-chondrites are similar in bulk major chemistry, there are significant differences between them. Firstly, Y-791493 is more abundant in metal than the average H-chondrite. Secondly, X_{Mg} of Y-791493 (0.896) is higher than that of the average H-chondrite (0.78). Figure 11 shows the relationship of X_{Mg} of olivine, orthopyroxene, and clinopyroxene. The plotted data are the average for the O-chondrites (VAN SCHMUS, 1969). Their Mg-Fe exchange equilibrium was maintained and they are more magnesian than those in H-chondrites, reflecting high

Table 6. Comparison of bulk chemical composition, their silicate portions, and mineral compositions of Y-791493, Lodran, Acapulco, ALH-77081, and the average H-chondrite.

	Y-791493[1]	Lodran[2]	Acapulco[3]	ALH-77081[4]	Ave. H[5]
SiO_2	36.07	34.9	37.55	40.87	35.64
TiO_2	0.05	0.16	0.13	tr.	0.14
Al_2O_3	0.93	0.44	2.25	2.27	2.00
FeO	6.33	6.4	6.38	4.98	11.71
MnO	0.43	0.33	0.38	0.39	0.28
MgO	30.52	24.9	24.71	26.0	23.73
CaO	1.59	0.8	1.57	0.83	1.76
Na_2O	0.22	0.04	0.83	1.01	0.73
K_2O	—	0.002	0.05	0.08	0.08
Cr_2O_3	0.84	0.57	0.74	0.72	0.46
P_2O_5	0.51	—	0.86	—	0.23
Fe	19.13	28.5*	20.3	14.6	15.8
Ni	1.14	2.24	2.2	1.6	1.70
Co	0.07	0.12	0.12	0.08	0.074
FeS	2.17	—	3.6	8.1	5.45
Silicate portion (100% recalculated)					
SiO_2	46.6	50.9	49.8	53.0	46.5
TiO_2	0.06	0.23	0.17	—	0.13
Al_2O_3	1.20	0.64	2.98	2.94	2.61
FeO	8.17	9.34	8.46	6.45	15.3
MnO	0.55	0.48	0.56	0.51	0.36
MgO	39.4	36.3	32.8	33.7	30.9
CaO	2.05	1.17	2.08	2.05	2.27
Na_2O_3	0.28	0.06	1.10	1.31	0.95
K_2O	—	0.003	0.06	0.11	0.10
Cr_2O_3	1.08	0.83	0.98	0.93	0.60
P_2O_5	0.66	—	1.14	—	0.30
Mg/(Mg+Fe)	0.896	0.874	0.873	0.903	0.780
Mineral compositions					
Ol (Fo)	87–91	88–91	88	89	81
Opx (En)	86–85	84	87–86	87	82
(Wo)	3.2–1.5	2.6	1.6	1.7	1.6
Cpx (En)	50–47	50	55	52–50	49
(Wo)	45–46	43	41	45–44	45
Pl (An)	16–18	—	14	15	12
(Or)	2–3	—	4	4	6
Sp (Cr_2O_3)	66–59	69–58	62	61.5	56.9
(MnO)	1.6–1.0	1.5–0.7	1.3	2.5	0.9
Kama (Ni)	6.5–6.7	7.5>Ni>6.4	5–6	6–6.6	6.4

(1) This study and HARAMURA *et al.* (1983), all Fe_2O_3 as Fe, volatile-free, (2) BILD and WASSON (1976); PRINZ *et al.* (1978); FUKUOKA *et al.* (1978), (3) PALME *et al.* (1981), (4) MASON (1978); TAKEDA *et al.* (1980), (5) HARAMURA *et al.* (1983); VAN SCHMUS (1969); BUNCH *et al.* (1976); AFIATALAB and WASSON (1980).

* Appears to contain FeS.

bulk X_{Mg}. Higher X_{Mg} of bulk chemistry and silicates and higher Fe/Ni ratio of Y-791493 compared with the average H-chondrite suggest that melting occurred under more reducing conditions than that of the average H-chondrite. Figure 11 also shows

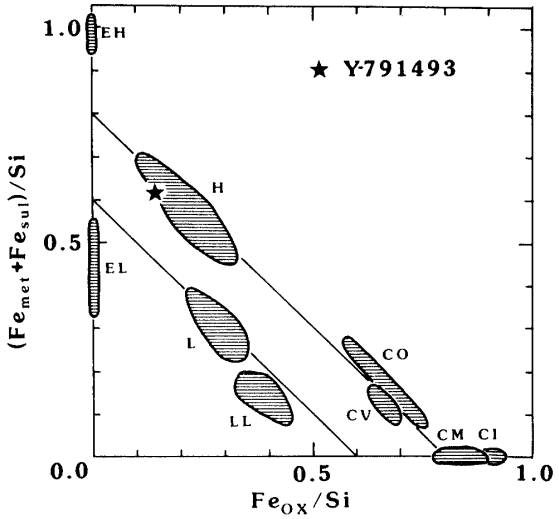

Fig. 10. Relation between $(Fe_{met}+Fe_{sul})/Si$ (atomic ratio) and Fe_{ox}/Si of Y-791493 and various chondrites. Fe_{met}, Fe_{sul}, and Fe_{ox} are Fe in metal, in sulfide, and in oxides, respectively. After WASSON (1985).

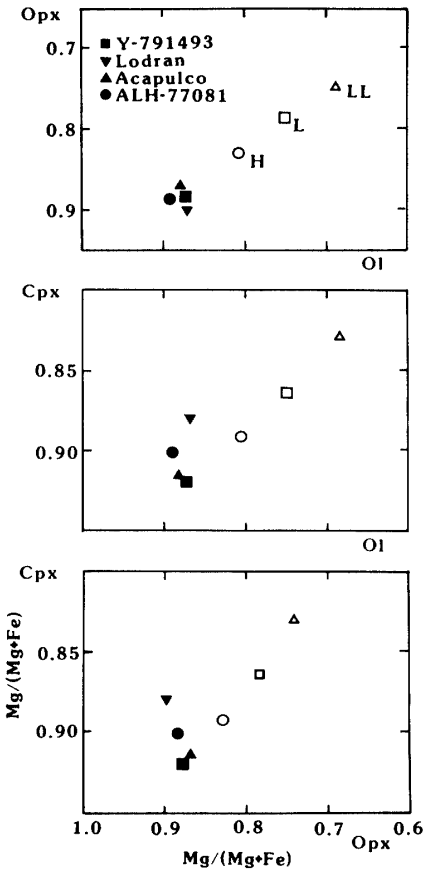

Fig. 11. Partition of Mg and Fe among olivine, orthopyroxene and clinopyroxene of Y-791493, Lodran, Acapulco, ALH-77081, and type 6 ordinary chondrites. Data from BUNCH and OLSEN (1973), BILD and WASSON (1976), TAKEDA et al. (1980), PALME et al. (1981), and VAN SCHMUS (1969).

that olivine, orthopyroxene, and clinopyroxene in Y-791493 are almost equilibrated and that the effect of selective reduction of olivine after crystallization was scarce or very small if any.

The bulk and mineral compositions of Y-791493 cannot be derived by partial melting of the average H-chondrite. The silicate portion of Y-791493 is depleted in TiO_2, Al_2O_3, Na_2O, CaO, and K_2O and enriched in Cr_2O_3, MnO, and P_2O_5 compared with the silicate portion of H-chondrites. Depletion of Ti, Al, Na, Ca, and K and enrichment of Cr are the results of partial melting and loss of the partial melt, which is well observed in the variation of the bulk composition of terrestrial residual peridotites (*e.g.*, MAALØE and AOKI, 1977). Enrichment of MnO by an FeO decrease due to reduction (TAKEDA *et al.*, 1980; GOODRICH and BERKLEY, 1985) is not the case with Y-791493 either, because the Mn/Mg ratio of Y-791493 is larger than that of the average H-chondrite. Thus the precursor material of Y-791493 should have been more enriched in Mn and P than the average H-chondrite.

The enrichment of Mn in Y-791493 is supported by the chemical composition of minerals. The mineral compositions also show depletion of TiO_2 and Na_2O and enrichment of Cr_2O_3 compared with the average H-chondrite as shown by the bulk chemical composition. Figure 12 shows the relationship between Cr_2O_3 content in spinel and anorthite mole% in plagioclase. Spinel in Y-791493 is more Cr_2O_3-rich and its plagioclase is more An-rich than those in H-chondrites. Figure 13A shows the relationship between Cr_2O_3 and TiO_2 content in spinel. Spinel in Y-791493 is poorer in TiO_2 and richer in Cr_2O_3 than that in ordinary chondrites. On the contrary, as shown in Fig. 13B spinel in Y-791493 is richer in MnO than that in ordinary chondrites. The MnO and Cr_2O_3 contents in spinel show a positive correlation with those in pyroxenes (Fig. 14A), indicating that the chemistry of spinel reflects the bulk chemical composition.

Metal-sulfide melt may have been distributed as small globules between crystals and they were sustained by large olivine and orthopyroxene crystals. TAKAHASHI (1983) carried out melting experiments on an L3 chondrite under high pressures (6–30 kbar) and showed that the eutectic melt of metal-sulfide existed as isolated patches dispersed between solid silicates below the silicate solidus temperature and as globules at higher temperatures. At higher temperatures, metal-sulfide globules were surrounded by the silicate melt and coalescence of globules rarely occurred at 15 kbar and 1400°C up to 10 hours. As a result, gravitational separation of metal-sulfide melt, silicates and silicate melt did not occur effectively. In the case of Y-791493, in addition to the low degree of melting, the low gravity of the probably small parental body did not promote the separation of metal-sulfide. Loss of partial melt was relatively easier as shown also by the experiments of TAKAHASHI (1983).

6.4. Other related meteorites

Y-791493 shows an intimate relationship to Lodran, Acapulco, and ALH-77081. Though the bulk chemical composition and modal composition of these meteorites are slightly different, they show many common chemical features; 1) compositions of the constituent minerals are similar, 2) they have high Mn, Cr, and P contents, and 3) oxygen isotopic compositions of Lodran and Acapulco are quite similar (CLAYTON

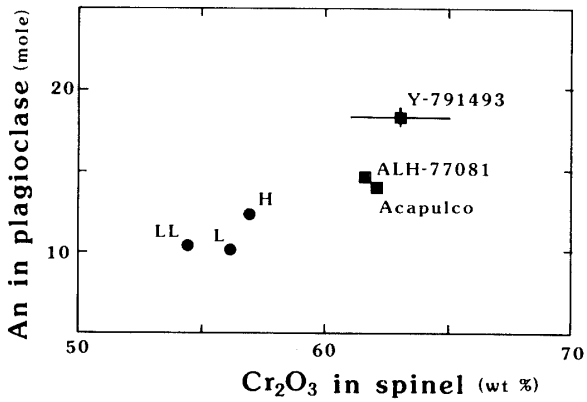

Fig. 12. Relationship between Cr_2O_3 in spinel and anorthite in plagioclase (mole) of Y-791493, Acapulco, ALH-77081, and type 6 ordinary-chondrites. Data from VAN SCHMUS (1969), BUNCH et al. (1976), TAKEDA et al. (1980), and PALME et al. (1981).

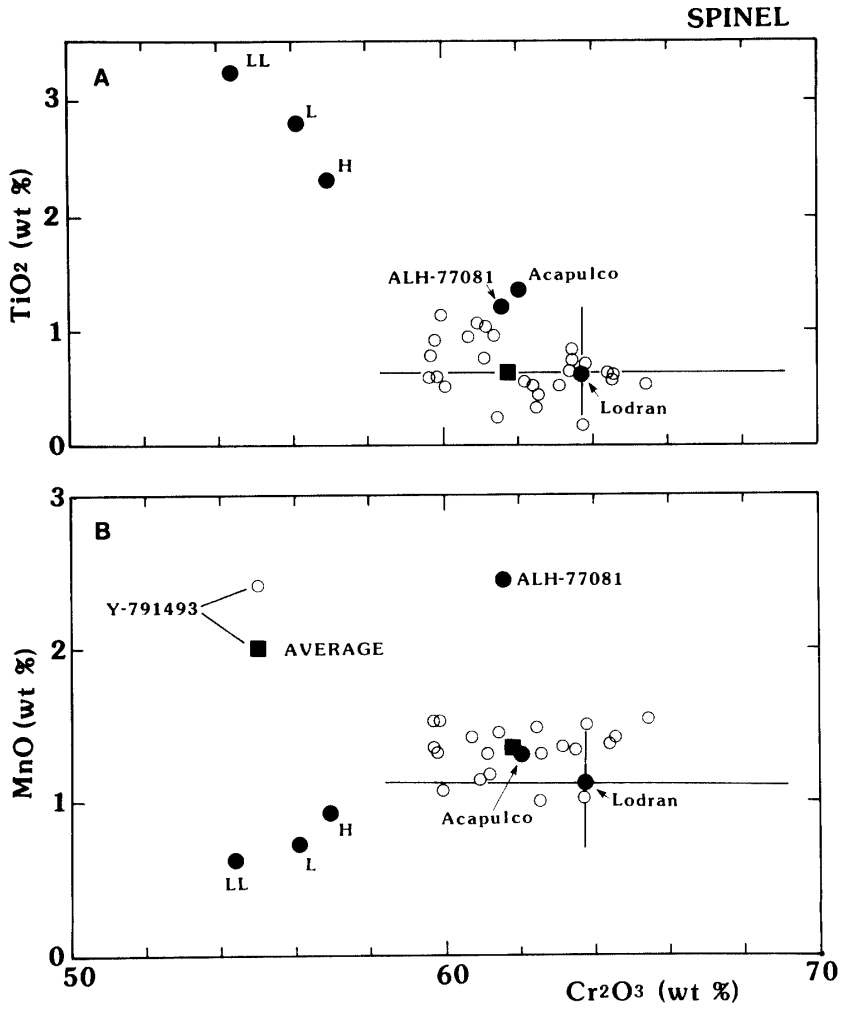

Fig. 13. Relationship between Cr_2O_3 and TiO_2 (A) and MnO (B) in spinel in Y-791493, Lodran, Acapulco, ALH-77081 and type-6 ordinary-chondrites. Data from VAN SCHMUS *(1969),* BILD *and* WASSON *(1976),* TAKEDA *et al. (1980) and* PALME *et al. (1981).*

and MAYEDA, 1978; MAYEDA and CLAYTON, 1980). As PRINZ *et al.* (1980, 1983) have pointed out, these meteorites may be related to "winonaites", Brachina, and silicates in IAB and IIICD irons. In Fig. 11, the relationship of X_{Mg} among olivine, orthopyroxene, and clinopyroxene in the former four meteorites is shown with those of ordinary chondrites. The homogeneous core compositions of Y-791493 and related meteorites are shown in the figure. They are essentially the same, indicating that X_{Mg} of olivine, orthopyroxene, and clinopyroxene were nearly in equilibrium at a certain stage of cooling. As they coexist with metallic iron, their compositions are controlled by the oxygen fugacity of the environment. This shows that these meteorites were formed under very similar oxygen fugacities.

Contents of minor elements in these four meteorites are very similar. Olivine and orthopyroxene contain characteristically high MnO (about 0.6 wt%) with lesser amounts of other minor elements. Clinopyroxenes are characterized by high Cr_2O_3 contents (1–1.5 wt%) (Fig. 12). Spinels are rich in Cr_2O_3 (Fig. 12) and MnO with

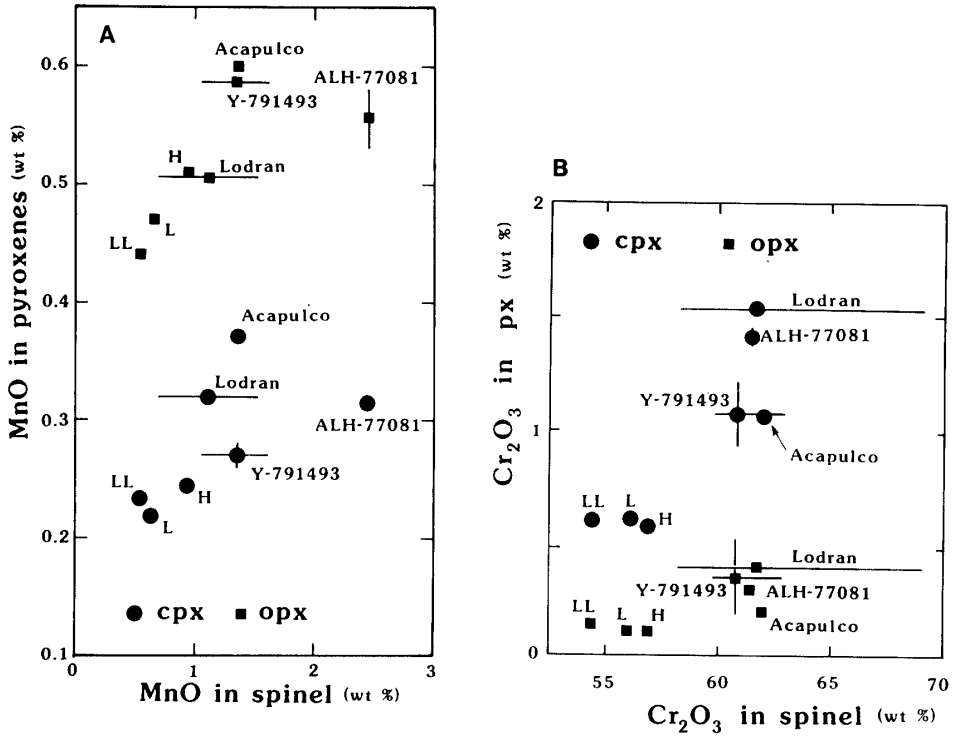

Fig. 14. Relationship between MnO (A) and Cr_2O_3 (B) in spinel, orthopyroxene, and clinopyroxene in Y-791493, Lodran, Acapulco, ALH-77081 and type 6 ordinary-chondrites. Data from VAN SCHMUS *(1969),* BILD *and* WASSON *(1976),* BUNCH *et al. (1976),* TAKEDA *et al. (1980), and* PALME *et al. (1981).*

significant amounts of ZnO (up to 2 wt%) which is also the case for "winonaites" and silicate inclusions in IAB and IIICD irons as PRINZ *et al.* (1980, 1983) have already pointed out. Plagioclases are relatively rich in anorthite and poor in orthoclase components compared with those in ordinary chondrites (Fig. 12). As a result of high Cr_2O_3 and MnO contents in major constituent minerals (Fig. 14), MnO and Cr_2O_3 contents in bulk meteorites are high. Though no P_2O_5 content was reported for Lodran and ALH-77081, Acapulco (0.86 wt%) and Y-791493 (0.51 wt%) are extremely rich in P_2O_5 (Table 6). Again, this may be the result of high Mn and P contents in the precursor material.

MASON (1978) noted the mineralogical and structural similarities between ALH-77081 and Acapulco. PALME *et al.* (1981) have pointed out the similar Fa contents in olivine and high bulk Cr_2O_3 contents in Lodran, Acapulco, and ALH-77081 and discussed the genetic association of these meteorites. The Cr_2O_3 content in Lodran is slightly lower than that in the other three meteorites which was also pointed out by FUKUOKA *et al.* (1978). PALME *et al.* (1981) suggested that Acapulco was formed from parental material similar to that of H-chondrites but more reduced and incipient melting. Lodran is considered to have been formed from a precursor material, hybrid between H- and E-chondrites through a limited partial melting (FUKUOKA *et al.*, 1978). PRINZ *et al.* (1983) have pointed out that the silicates in IAB and IIICD irons, "winonaites", "lodranites", and Brachina are mineralogically and chemically related and that they were formed through minor but different degree of partial melting of

chondritic materials.

Extremely similar mineral compositions for all constituents and similar proposed formation mechanisms indicate that Y-791493, Acapulco, ALH-77081, and Lodran originated from the same precursor in the same parental body. The Cr_2O_3 contents in spinel and clinopyroxene are the highest in Lodran (Fig. 14B) indicating that the degree of melt extraction was the highest in Lodran among these four meteorites. This is consistent with the fact that Lodran lacks plagioclase and is poor in clinopyroxene as an interstitial phase. As shown in Fig. 12, plagioclase in Y-791493 is the most An-rich among those three meteorites. Further, the Or content in Y-791493 is a little lower than that in the other three meteorites, which indicates higher degree of loss of partial melt of Y-791493 than for Acapulco and ALH-77081. The difference in An and Or contents of plagioclase of the three related meteorites shows that the degree of melt extraction for Y-791493 was higher than that in Acapulco and ALH-77081, which were similar.

Lodran, Y-791493, Acapulco and ALH-77081 were formed from the same precursor material through different degrees of melting, the degree of melting decreasing in this order. Isotopic compositions of Y-791493 and ALH-77081 are not yet known. Measurement of oxygen isotopic compositions of Y-791493 and ALH-77081 will be required in order to further clarify their genetical relationship to Lodran and Acapulco.

Acknowledgments

We are grateful to the National Institute of Polar Research for the loan of the polished thin section, to the Ocean Research Institute of University of Tokyo for the use of EPMA (cooperative number 84146), and to the National Museum of Natural Sciences for the use of SEM-EDS. We thank the EPMA Application Laboratory of Electron Optics Technical and Engineering Division of JEOL for the CMA analysis. We thank I. KUSHIRO, M. TORIUMI, and A. ISHIWATARI for discussions. Thorough reviews by M. PRINZ, H. PALME, and J. JONES greatly helped to improve the manuscript. One of the authors (H.N.) gratefully acknowledges Inoue Fundation for Science for the research aid. This study was supported by grant-in-aid 60740461 from the Ministry of Education, Science and Culture, Japan.

References

AFIATTALAB, F. and WASSON, J. T. (1980): Composition of metal phases in ordinary chondrites; Implications regarding classification and metamorphism. Geochim. Cosmochim. Acta, **44**, 431–446.

BENCE, A. E. and ALBEE, A. L. (1968): Empirical correction factors for the electron microanalysis of silicates and oxides. J. Geol., **76**, 382–403.

BERKLEY, J.L. and KEIL, K. (1981): Olivine orientation in the ALHA77005 achondrite. Am. Mineral., **66**, 1233–1236.

BERKLEY, J. L., TAYLOR, G. J. and KEIL, K. (1980): The nature and origin of ureilites. Geochim. Cosmochim. Acta, **44**, 1579–1597.

BILD, R. W. (1977): Silicate inclusions in group IAB irons and a relation to the anomalous stones Winona and Mt. Morris (Wis). Geochim. Cosmochim. Acta, **41**, 1439–1456.

BILD, R. W. and WASSON, J. T. (1976): The Lodran meteorite and its relationship to the ureilites.

Mineral. Mag., **40**, 721–735.

BROTHERS, R. N. (1959): Flow orientation of olivine. Am. J. Sci., **257**, 574–584.

BUNCH, T. E. and OLSEN, E. (1973): Ortho-clinopyroxene compositions in ordinary chondrites and related Blander model calculation procedures. NASA Tech. Memo. NASA TMX-62, **259**, 16 p.

BUNCH, T. E., KEIL, K. and SNETSINGER, K. G. (1976): Chromite composition in relation to chemistry and texture of ordinary chondrites. Geochim. Cosmochim. Acta, **31**, 1569–1582.

BUSECK, P. R. (1977): Pallasite meteorites—mineralogy, petrology and geochemistry. Geochim. Cosmochim. Acta, **41**, 711–740.

CLAYTON, R. N. and MAYEDA, T. K. (1978): Genetic relations between iron and stony meteorites. Earth Planet. Sci. Lett., **40**, 168–174.

DICK, H. J. B. and BULLEN, T. (1984): Chromian spinel as a petrogenetic indicator in abyssal and alpine-type peridotites and spatially associated lavas. Contrib. Mineral. Petrol., **86**, 54–76.

FUKUOKA, T., Ma, M.-S., WAKITA, H. and SCHMITT, R. A. (1978): Lodran; The residue of limited partial melting of matter like a hybrid between H and E chondrites. Lunar and Planetary Science IX. Houston, Lunar Planet. Inst., 356–358.

GOODRICH, C. A. and BERKLEY, J. L. (1985): Minor elements in ureilites; Evidence for reverse fractionation and interstitial silicate liquids. Lunar and Planetary Science XVI. Houston, Lunar Planet. Inst., 280–281.

GRAHAM, A. L., EASTON, A. J. and HUTCHISON, R. (1977): Forsterite chondrites; The meteorites Kakangari, Mount Morris (Wisconsin), Pontlyfni, and Winona. Mineral. Mag., **41**, 201–210.

HARAMURA, H., KUSHIRO, I. and YANAI, K. (1983): Chemical compositions of Antarctic meteorites I. Mem. Natl Inst. Polar Res., Spec. Issue, **30**, 109–121.

HUANG, W. T. and MERRITT, C. A. (1952): Preferred orientation of olivine crystals in troctolite of the Wichita Mountains, Oklahoma. Am. Mineral., **37**, 865–868.

IRVING, A. J. (1978): A review of experimental studies of crystal/liquid trace element partitioning. Geochim. Cosmochim. Acta, **42**, 743–770.

JAQUES, A. L. and GREEN, D. H. (1980): Anhydrous melting of peridotite at 0–15 kb pressure and the genesis of tholeiitic basalts. Contrib. Mineral. Petrol., **73**, 287–310.

LINDSLEY, D. H. and ANDERSEN, D. J. (1983): A two-pyroxene thermometer. Proc. Lunar Planet. Sci. Conf., 13th, Pt. 2, A887–A906 (J. Geophys. Res., **88** Suppl.).

MAALØE, S. and AOKI, K. (1977): The major element composition of the upper mantle estimated from the composition of lherzolites. Contrib. Mineral. Petrol., **63**, 161–173.

MASON, B. (1978): Antarctic meteorite data sheet; Sample No. 30081. Antarct. Meteorite Newsl., **1**, 19.

MATSUMOTO, Y., YANAI, K. and KOJIMA, H. (1983): A stony-iron meteorite; Yamato-75274 (abstract). Papers presented to the Eighth Symposium on Antarctic Meteorites, 17–19 February 1983. Tokyo, Natl Inst. Polar Res., 6.

MAYEDA, T. K. and CLAYTON, R. N. (1980): Oxygen isotopic compositions of aubrites and some unique meteorites. Proc. Lunar Planet. Sci. Conf., 11th, 1145–1151.

MYSEN, B. O. and KUSHIRO, I. (1977): Compositional variations of coexisting phases with degree of melting of peridotite in the upper mantle. Am. Mineral., **62**, 843–865.

NAGAHARA, H. and OZAWA, K. (1985): Yamato-791493, "lodranite" (abstract). Papers presented to the Tenth Symposium on Antarctic Meteorites, 25–27 March 1985. Tokyo, Natl Inst. Polar Res., 194–197.

NARAYAN, C. and GOLDSTEIN, J. I. (1985): A major revision of iron meteorite cooling rates—An experimental study of the growth of the Widmanstätten pattern. Geochim. Cosmochim. Acta, **49**, 397–410.

OZAWA, K. (1983): Evaluation of olivine-spinel geothermometry as an indicator of thermal history for peridotites. Contrib. Mineral. Petrol., **82**, 52–65.

OZAWA, K. (1984): Olivine-spinel geospeedometry; Analysis of diffusion-controlled Mg-Fe^{2+} exchange. Geochim. Cosmochim. Acta, **48**, 2597–2611.

PALME, H., SCHULTZ, L., SPETTEL, B., WEBER, H. W., WÄNKE, H., CHRISTOPHE MICHEL-LEVY, M. and LORIN, J. C. (1981): The Acapulco meteorite; Chemistry, mineralogy and irradiation effects. Geochim. Cosmochim. Acta, **45**, 727–752.

PRINZ, M., KLIMENTIDIS, R., HARLOW, G. E. and HEWINS, R. H. (1978): Petrologic studies on the origin of the Lodran meteorite. Lunar and Planetary Science IX. Houston, Lunar Planet. Inst., 919–921.

PRINZ, M., WAGGONER, D. G. and HAMILTON, P. J. (1980): Winonaites; A primitive achondritic group related to silicate inclusions in IAB irons. Lunar and Planetary Science XI. Houston, Lunar Planet. Inst., 902–904.

PRINZ, M., NEHRU, C. E., DELANEY, J. S. and WEISBERG, M. (1983): Silicates in IAB and IIICD irons, winonaites, lodranites and Brachina; A primitive and modified-primitive group. Lunar and Planetary Science XIV. Houston, Lunar Planet. Inst., 616–617.

PRIOR, G. T. (1916): On the genetic relationship and classification of meteorites. Mineral. Mag., **18**, 26–44.

TAKAHASHI, E. (1983): Melting of a Yamato L3 chondrite (Y-74191) up to 30 kbar. Mem. Natl Inst. Polar Res., Spec. Issue, **30**, 168–180.

TAKEDA, H., MORI, H., YANAI, K. and SHIRAISHI, K. (1980): Mineralogical examination of the Allan Hills achondrites and their bearing on the parent bodies. Mem. Natl Inst. Polar Res., Spec. Issue, **17**, 119–144.

VAN SCHMUS, W. R. (1969): The mineralogy and petrology of chondritic meteorites. Earth Sci. Rev., **5**, 145–184.

WASSON, J. T. (1974): Meteorites; Classification and Properties. Berlin, Springer, 316 p.

WASSON, J. T. (1985): Meteorites; Their Record of Early Solar-system History. New York, Freeman, 267 p.

YANAI, K. and KOJIMA, H. (1982): A lodranite in the Yamato collections (abstract). Meteoritics, **17**, 300.

YANAI, K. and KOJIMA, H. (1983): A new stony-iron meteorite collection in the Yamato meteorites (abstract). Meteoritics, **18**, 429.

YANAI, K., KOJIMA, H., PRINZ, M., NEHRU, C. E., WEISBERG, M. K. and DELANEY, J. S. (1984): Petrologic studies of three primitive achondrites from the Yamato meteorites collection, Antarctica (abstract). Papers presented to the Ninth Symposium on Antarctic Meteorites, 22–24 March 1984. Tokyo, Natl Inst. Polar Res., 24–28.

YOSHINO, G. (1961): Structural-petrological studies of peridotite and associated rocks of the Higashiakaishi-yama district, Shikoku, Japan. J. Sci. Hiroshima Univ., Ser. C, 343–402.

(Received August 22, 1985; Revised manuscript received November 27, 1985)